Boundaries of Operation for Refurbished Parallel AC–DC Reconfigurable Links in Distribution Grids

Shekhar, Aditya; Ramirez Elizondo, Laura; Soeiro, Thiago B.; Bauer, Pavol

Important note
To cite this publication, please use the final published version (if applicable).
Please check the document version above.

Boundaries of Operation for Refurbished Parallel AC-DC Reconfigurable Links in Distribution Grids

Aditya Shekhar, Laura Ramírez-Elizondo, Thiago Batista Soeiro and Pavol Bauer

Abstract—Parallel ac-dc reconfigurable link technology can find interesting applications in medium voltage power distribution. A given system can operate in different configurations while maintaining equivalent capacity during (n-1) contingencies using reconfigurability. This paper provides a method for the ideal selection of the link configuration by defining the efficiency and economic viability boundaries with varying operating power demand and power factor. A sensitivity analysis with parameters such as grid voltage, link length, conductor area and converter efficiency as well as economic factors such as converter cost and link conductor installation cost is discussed. The study identifies the operating zones wherein the refurbished parallel ac-dc reconfigurable distribution links can be an efficient and economically preferred option of delivering power as compared to a system with only ac or dc links.

Index Terms—capacity enhancement, dc links, distribution network, efficiency, flexible, medium voltage, reconfiguration

NOMENCLATURE

A_{con}	Link conductor area.
C0	Benchmark system with only ac conductors.
Cn	Refurbished system configuration; where, n can take integer values between 1 to $\frac{N_{ori}}{3}$.
$i_{Cn,ac}$	single ac conductor current for configuration Cn.
$i_{Cn,dc}$	single dc conductor current for configuration Cn.
L, L_{link}	Distance between sending and receiving substation.
$L_{C2,max}$	Maximum L_{link} at which configuration C2 is the most efficient.
$L_{C2,min}$	Minimum L_{link} at which configuration C2 is the most efficient.
$L_{cr,C0Cn}$	Link length above which configuration Cn is more efficient than C0.
$L_{10,C0-C2}$	Minimum L_{link} for which the payback of C2 as compared to C0 is lower or equal to 10 years.
$L_{10,C1-C2}$	Maximum L_{link} for which the payback of C2 as compared to C1 is lower or equal to 10 years.
$N_{ac,Cn}$	Number of ac conductors for configuration Cn.
$N_{dc,Cn}$	Number of dc conductors for configuration Cn.
N_{ori}	Total number of link conductors.
N_{red}	Number of redundant conductors.
$P_{cond,Cn}$	Link conductor power loss for configuration Cn.
$P_{conv,Cn}$	Converter power loss for configuration Cn.
$P_{loss,Cn}$	Total power loss for configuration Cn.
$r_{Cn,ac}$	single ac conductor resistance in Ω/km for Cn.
$r_{Cn,dc}$	single dc conductor resistance in Ω/km for Cn.
$S_{max,ac}$	Maximum power capacity of ac link.
$S_{max,dc}$	Maximum power capacity of dc link.
S_{link}	Power capacity of a single link in the system.
S_{RSS}	Apparent power demand at receiving substation.
$S_{conv,RSS}$	Apparent power of the receiving end converter.
$S_{conv,SSS}$	Apparent power of the sending end converter.
$T_{Cn,ac}$	Single ac conductor temperature for Cn.
$T_{Cn,dc}$	Single dc conductor temperature for Cn.
$V_{LL,rms}$	line to line r.m.s. substation ac bus voltage.
V_{dc}	Voltage of the dc link.
y	ratio of active dc power flow to that of the total active power demand at system receiving end.
y_{min}, y_{max}	Minimum and maximum y, respectively.
η_{RSS}	Efficiency of the receiving substation converter.
η_{SSS}	Efficiency of the sending substation converter.
θ	phase angle at receiving end for power factor $\cos\theta$.

I. INTRODUCTION

An impending challenge faced by the distribution network operators (DNOs) is that of the increasing energy demand. For example, if the currently used gas based heating systems in The Netherlands are replaced by electric heaters, the demand from the grid will grow. Similarly, larger market penetration of high power consumers such as electric vehicles can result in a shortage of required power delivery capacity. In such situations, restructuring the existing ac grid infrastructure using flexible dc links can be an interesting solution for the necessary capacity enhancement [1]–[3]. The concept of converting the existing ac links for refurbished dc operation to maximize the power transfer capacity has recently gained significant attention [4]–[7].

It was shown in [4] that the total capacity of underground ac cables can be improved by at least 1.5 times if they are refurbished to operate under dc conditions under specified assumptions. The field implementation of renovated dc operation for capacity upgradation of XLPE cable line showed four years of uninterrupted operation with economic and reliability benefits as compared to the ac solution [5]. The study anticipated significant increase in achievable capacity gains and recommended a gradual rise in the operating dc link voltage with growing experience about the system. Similar or higher enhancement is possible if the system involves overhead lines [7], [8]. Superior efficiency of the employed ac/dc power electronic devices ensured that some efficiency gains over the original system are also achievable. Due to modularity, scalability, better harmonic performance and higher efficiency,

half bridge ac/dc modular multilevel converters (MMC) [9]–[11] were chosen for the proposed high power medium voltage dc link operation.

The contingency analysis of such a refurbished dc system indicated that during fault conditions, some level of architecture reconfigurability is necessary to maintain the enhanced capacity [12]. The developed reconfigurable parallel ac-dc system is described in greater detail in Section II. In [13], it was highlighted that during healthy conditions, the same system can be operated under different physical configurations while maintaining the same capacity during (n-1) contingencies. It was further highlighted that the selection of the best possible configuration requires the quantification of trade-offs related to cost, efficiency and reliability.

Among the earliest accounts of parallel operation of ac and dc lines for high voltage power transmission is found in [14]. In this work, greater flexibility of dc transmission as well as rapid control were considered advantageous for the composite system operation. Considering the effective conductor utilization with dc operation, in addition to the stability benefits, simultaneous operation of ac and dc in the same link is proposed in [15]. Some challenges of parallel ac-dc system were explored in [16]. Over the years, the power system apparatus, corresponding device capabilities as well as grid requirements have significantly changed [17]. Consequently, the application of parallel ac-dc power delivery concept has broadened. Recognizing the advantage of using dc alongside ac distribution, authors in [18] proposed a unified load flow model applicable to hybrid radial networks with distributed resources. The optimal operation of hybrid ac-dc power distribution is explored in [19], [20]. An interesting recent research aims at interconnecting Crete island to Greek mainland using parallel ac-dc links [21], [22]. The project explored the ability of these interconnectors for ensuring the continuity of supply, while minimizing the use of local generation in maintaining the capacity during (n-1) contingency. The operating boundaries wherein a parallel ac-dc link is advantageous as compared to a purely ac or a purely dc system of equivalent capacity is less explored in the literature.

The focus of this paper is to prove that reconfigurable parallel ac-dc links can be an efficient and economically preferred option, particularly for delivering high power (few tens of MVA) at medium voltage levels (one to few tens of kV) for short distances (0-50 km). The specific contributions are as followed:

- Developing a generalized approach describing the possible system configurations and their capacity constraints.
- Establishing the equations describing the system losses under different configurations.
- Defining the efficiency boundaries for a case-study with varying link lengths, power demand and power factor.
- Performing the sensitivity analysis to describe the variation in the defined boundaries with grid voltage, link conductor area and average efficiency of station converter.
- Presenting an economic analysis of the payback of added investment associated with different configurations.

II. GENERALIZED DESCRIPTION OF RECONFIGURABLE PARALLEL AC-DC LINK SYSTEM

A. System Description

Let us consider that the Sending end Sub-Station (SSS) and the Receiving end Sub-Station (RSS) of an overloaded benchmark ac link system are interconnected using a specified number of conductors (equal to N_{ori}). In order to enhance the capacity during (n-1) contingencies, this system is refurbished to form a reconfigurable parallel ac-dc link as shown in Fig 1.
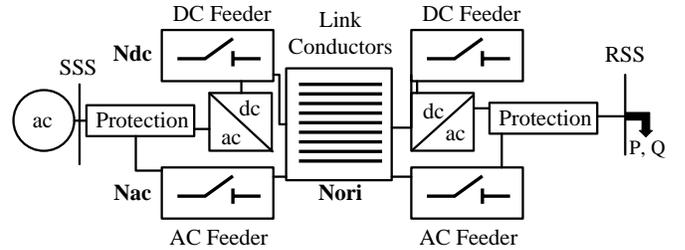

Fig. 1: Refurbished parallel ac-dc reconfigurable links in distribution grids.

The power flow between SSS and RSS is directed by the reconfiguration of switch blocks marked 'DC Feeder' and 'AC Feeder' that select the number of lines operating in dc and ac mode respectively. Depending on the combination of normally open (NO) and normally closed (NC) switches in these feeders, different system configurations are possible (see Section II-B). The reconfigurability is necessary if the required power delivery capacity is to be maintained during faults. However, it is important to select the best possible configuration during normal conditions to ensure the most efficient and economically viable system operation.

The link conductors can be either overhead lines or underground cables. Further, the cables can be single-cored or three-cored. The protection block at the ac side of each substation can be designed such that each ac or dc link acts as a point to point connection between SSS and RSS that can be isolated from ac side individually during faults. Alternatively, a common ac circuit breaker can be employed or dc breakers can also be explored [23]. Similarly, design choices are available for the ac/dc converter blocks used for the dc link operation. A detailed discussion on different architectures, various choices available and the associated trade-offs in terms of reliability, efficiency and cost is presented in [12], [13]. In this paper, the results are shown with assumptions corresponding to single-cored underground cables with multiple MMCs per substation.

B. Configuration Strategies

The pre-refurbished system originally operates as multiple 3-phase ac links, therefore, N_{ori} is a multiple of three, which is most commonly 6 or 9 to meet the necessary redundancy requirements. Depending on the state of the NO and NC switches in the feeders, different combinations of number of conductors operating in ac (N_{ac}) and dc (N_{dc}) are possible. N_{ac} is always a multiple of three for three phase ac implementation, while N_{dc} is even for a symmetric monopolar dc

link implementation [24]. With the goal of maximizing the link conductor utilization U_{cond}, the refurbished ac-dc system can operate in $\left(\frac{N_{\text{ori}}}{3}\right)$ possible configurations. In general, for any configuration 'Cn', the number of conductors operating in ac mode ($N_{\text{ac,Cn}}$) is given by (1).

$$N_{\text{ac,Cn}} = (n-1) * \left(\frac{N_{\text{ori}}}{3}\right) \tag{1}$$

Where, n can take integer values between 1 to $\frac{N_{\text{ori}}}{3}$. Correspondingly, the number of conductors operating in dc mode ($N_{\text{dc,Cn}}$) is given by (2).

$$N_{\text{dc,Cn}} = \begin{cases} N_{\text{ori}} - N_{\text{ac,Cn}}, & \text{if } N_{\text{ori}} - N_{\text{ac,Cn}} \text{ is even} \\ N_{\text{ori}} - N_{\text{ac,Cn}} - 1, & \text{otherwise} \end{cases} \tag{2}$$

The number of redundant conductors (N_{red}) during normal operation for any configuration is given by (3),

$$N_{\text{red}} = N_{\text{ori}} - (N_{\text{ac,Cn}} + N_{\text{dc,Cn}}) \tag{3}$$

Additionally, the benchmark configuration referred to as 'C0' in this paper, refers to the conventional solution where additional conductors are installed by the DNOs for capacity enhancement in the ac link system. Based on the results presented in [4], C0 needs approximately 1.5 times more conductor area than the configuration with complete dc operation for equivalent capacity during (n-1) contingencies. Therefore, the total number of conductors $N_{\text{ac,C0}}$ is given by (4).

$$N_{\text{ac,C0}} = 1.5 * N_{\text{dc,Cn}}, \text{when, } N_{\text{ac,Cn}} = 0 \tag{4}$$

An example of possible configurations and corresponding number of conductors for $N_{\text{ori}} = 9$ is shown in Table I.

TABLE I: Number of ac, dc & redundant conductors under operation for different configuration strategies with $N_{\text{ori}} = 9$.

	C0	C1	C2	C3
N_{ac}	12	0	3	6
N_{dc}	0	8	6	2
N_{red}	0	1	0	1

For a given N_{ori}, there are $\left(\frac{N_{\text{ori}}}{3} + 1\right)$ possible architectures with the same power delivery capacity during (n-1) contingencies. Each configuration has a different efficiency and economic consideration, depending on the link length 'L'; per km conductor resistance 'r_{Cn}' corresponding to cross-sectional area A_{con} and temperature T_{Cn}; conductor current i_{Cn} corresponding to the power demand, dc to ac voltage and power ratio; power factor (pf); and the converter efficiency η. The paper will describe both efficiency and economic viability boundaries based on the sensitivity of the system to the above mentioned parameters and offer insight on how to select the best possible configuration.

C. Power delivery capacity constraints

For a given configuration C_{n}, there are $\frac{N_{\text{ac,Cn}}}{3}$ three phase ac links and $\frac{N_{\text{dc,Cn}}}{2}$ dc links. The associated maximum power transfer capacities during normal operation, $S_{\text{max,ac}}$ and $S_{\text{max,dc}}$, are given by (5) and (6) respectively.

$$S_{\text{max,ac}} = \frac{N_{\text{ac,Cn}}}{3} \cdot S_{\text{link}} \tag{5}$$

$$S_{\text{max,dc}} = \frac{N_{\text{dc,Cn}}}{2} \cdot S_{\text{link}} \tag{6}$$

Where, S_{link} is the capacity of an individual link in the system, which can be assumed approximately equal for a three conductor ac link and a two conductor dc link [4]. This simplification is based on the assumption that the dc voltage imposed on any link conductor is $\sqrt{2}$ times the ac grid phase voltage [25].

The configurations employing parallel ac-dc links have an additional degree of freedom in controlling the active power flow using the dc link converters. The ratio of active dc power flow to that of the total active power demand at the RSS is defined as 'y' and this can influence the efficiency of the system in meeting the given apparent power demand at the RSS (S_{RSS}). At pf=1, the minimum y_{min} and maximum y_{max} are given by (7) and (8), respectively.

$$y_{\text{min}} = \begin{cases} 0, & \text{if } S_{\text{RSS}} \leq S_{\text{max,ac}} \\ \frac{S_{\text{RSS}} - S_{\text{max,ac}}}{S_{\text{RSS}}}, & \text{otherwise} \end{cases} \tag{7}$$

$$y_{\text{max}} = \begin{cases} 1, & \text{if } S_{\text{RSS}} \leq S_{\text{max,dc}} \\ \frac{S_{\text{max,dc}}}{S_{\text{RSS}}}, & \text{otherwise} \end{cases} \tag{8}$$

The precise value of these limits vary with pf, however it can be shown that this will not alter the efficiency boundaries under the operating conditions explored in this paper.

D. Conductor temperature and resistance

A range of ac and dc conductor currents, temperatures and resistances are possible for meeting the same apparent power demand, which influence the system level efficiency of each configuration. For a particular conductor current I_{cond}, the operating temperature $T_{\text{cond,k}}$ and conductor resistance $R_{\text{cond,k}}$ at k^{th} iteration is computed based on (9) and (10) respectively.

$$T_{\text{cond,k}} = T_{\text{amb}} + \left(\frac{I_{\text{cond}}^2 R_{\text{cond,k-1}}}{I_{\text{rated}}^2 R_{90°C}}\right)(90 - T_{\text{amb}}) \tag{9}$$

$$R_{\text{cond,k}} = R_{90°C}\left(\frac{1 + \alpha(T_{\text{cond,k}} - T_{\text{amb}})}{1 + \alpha(90 - T_{\text{amb}})}\right) \tag{10}$$

Herein, T_{amb} is the ambient temperature, $R_{90°C}$ is the resistance of the conductor in Ω/km at 90°C and α is the temperature coefficient. $R_{\text{Tcond,0}}$ is the initial conductor resistance assumed equal to R_{90C}. The iterative process terminates once the difference in the estimated resistance between two iterations becomes less than $1e^{-6}$.

E. Converter Losses

The theory presented in [26], [27] indicates that with increasing operating power and voltage, higher number of cascaded cells are favourable for optimal efficiency and performance at a given dc link voltage. Based on these concepts

it was shown that a half bridge medium voltage grid connected MMC with $3.3\,\mathrm{kV}$ Insulated Gate Bipolar Transistor (IGBT) switch based nine submodule cells is a reasonable design choice with high efficiency for this application [28]. The efficiency computations were performed based on the steady state analytical loss model described in [29] including switching, conduction and inductor losses and will not be repeated here in the interest of brevity. The percentage load dependent efficiency curve for a $10\,\mathrm{MVA}$ MMC operating at $313\,\mathrm{Hz}$ submodule switching frequency is shown in Fig. 2. The losses in the arm inductors corresponds to air-cored $3\,\mathrm{mH}$ inductance.
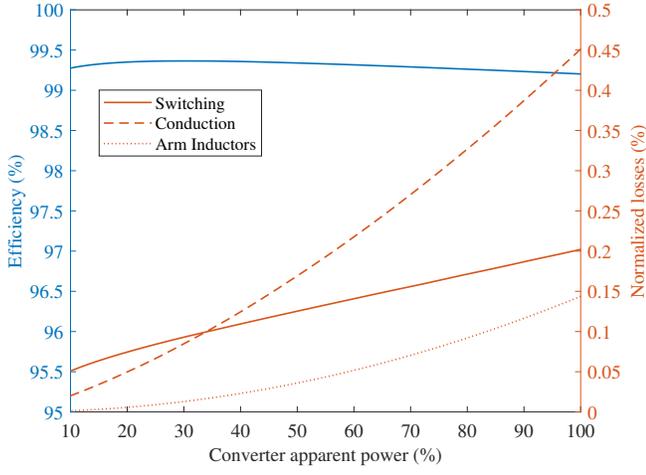

Fig. 2: Losses and Efficiency curve for DC Link modular multilevel converter with respect to loading.

This efficiency curve is adapted based on the considered full load capacity of the substation converters. Assuming that the reactive power demand at RSS is fully met by the substation converter, the RSS side converter demand $S_{\mathrm{conv,RSS}}$ is given by (11).

$$S_{\mathrm{conv,RSS}} = S_{\mathrm{RSS}}\sqrt{y^2\cos^2\theta + \sin^2\theta} \qquad (11)$$

At the SSS side, the converter supplies the dc link power and its demand $S_{\mathrm{conv,SSS}}$ is given by (12).

$$S_{\mathrm{conv,SSS}} = yS_{\mathrm{RSS}}\cos\theta \qquad (12)$$

Based on the converter demands described by (11) and (12) and the associated efficiency η described by Fig. 2, the total converter losses of the system can be calculated. It can be observed in Fig. 2 that the efficiency curve of the MMC is nearly flat for a wide range of percentage loading, and thus, assuming a constant efficiency can be a reasonable simplification. This is further important if several partially rated converters are employed per substation with optimal load sharing. Nevertheless, a sensitivity analysis of the described boundaries with varying efficiency will be explored.

F. System Losses for Different Configurations

For any N_{ori}, the system loss equations can take three possible structure corresponding to 1) complete ac configura-

tion (C0) 2) complete dc configuration (C1) 3) parallel ac-dc configurations (Cn with $n \neq (0, 1)$).

1) Configuration C0: The current per conductor (i_{C0}) is given by (13),

$$i_{\mathrm{C0}} = \frac{S_{\mathrm{RSS}}}{\left(\frac{N_{\mathrm{ac,C0}}}{3}\right)\sqrt{3}V_{\mathrm{LL,rms}}} = \frac{\sqrt{3}S_{\mathrm{RSS}}}{(N_{\mathrm{ori}}+3)V_{\mathrm{LL,rms}}} \qquad (13)$$

$V_{\mathrm{LL,rms}}$ is the line to line r.m.s. SSS bus voltage. The total link conductor loss $P_{\mathrm{loss,C0}}$ is given by (14),

$$P_{\mathrm{loss,C0}} = N_{\mathrm{ac,C0}}I_{\mathrm{C0}}^2 R_{\mathrm{C0}} = \frac{3S_{\mathrm{RSS}}^2 Lr_{\mathrm{C0}}(T_{\mathrm{C0}}, A_{\mathrm{con}})}{(N_{\mathrm{ori}}+3)V_{\mathrm{LL,rms}}^2} \qquad (14)$$

$r_{\mathrm{C0}}(T_{\mathrm{C0}}, A_{\mathrm{con}})$ is the ohmic ac resistance per kilometer depending on the operating conductor temperature T_{C0} and A_{con}.

2) Configuration C1: During normal operating conditions, the per conductor dc current i_{C1} that flows through each of the $\left(\frac{n_{\mathrm{dc,C1}}}{2}\right)$ dc links as given by (15).

$$i_{\mathrm{C1}} = \frac{S_{\mathrm{RSS}}\cos\theta}{\left(\frac{N_{\mathrm{dc,C1}}}{2}\right)V_{\mathrm{dc}}} = \sqrt{\frac{3}{2}}\left(\frac{S_{\mathrm{RSS}}\cos\theta}{V_{\mathrm{LL,rms}}N_{\mathrm{dc,C1}}}\right) \qquad (15)$$

where,

$$V_{\mathrm{dc}} = \frac{2\sqrt{2}V_{\mathrm{LL,rms}}}{\sqrt{3}} \qquad (16)$$

V_{dc} is the rated operating voltage of the dc link and $\cos\theta$ is the power factor of the load connected at the RSS. The total dc link conductor power loss $P_{\mathrm{cond,C1}}$ is given by (17).

$$P_{\mathrm{cond,C1}} = \frac{3S_{\mathrm{RSS}}^2\cos^2\theta Lr_{\mathrm{C1}}(T_{\mathrm{C1}}, A_{\mathrm{con}})}{2N_{\mathrm{dc,C1}}V_{\mathrm{LL,rms}}^2} \qquad (17)$$

Where, $r_{\mathrm{C1}}(T_{\mathrm{C1}}, A_{\mathrm{con}})$ is the dc conductor resistance in ohm per km depending on operating temperature T_{C1} and conductor area of cross-section. Based on Section II-E, the derived converter loss $P_{\mathrm{conv,C1}}$ is given by (18).

$$P_{\mathrm{conv,C1}} = S_{\mathrm{RSS}}[(1 - \eta_{\mathrm{SSS}})\cos\theta + (1 - \eta_{\mathrm{RSS}})] \qquad (18)$$

η_{SSS} and η_{RSS} is the efficiency of the SSS and RSS side converter stations. For C1, the value of y for computing the equations (11) and (12) is equal to 1. From (17) and (18), the total system losses $P_{\mathrm{loss,C1}}$ are estimated using (19),

$$P_{\mathrm{loss,C1}} = P_{\mathrm{cond,C1}} + P_{\mathrm{conv,C1}} \qquad (19)$$

3) Parallel ac-dc configurations Cn with $n \neq (0,1)$: There are $\left(\frac{N_{\mathrm{ori}}}{3} - 1\right)$ possible parallel ac-dc configurations with structurally similar loss equations. The corresponding dc and ac conductor currents, $i_{\mathrm{Cn,dc}}$ and $i_{\mathrm{Cn,ac}}$, are given by (20) and (21), respectively.

$$i_{\mathrm{Cn,dc}} = \frac{yS_{\mathrm{RSS}}\cos\theta}{\left(\frac{N_{\mathrm{dc,Cn}}}{2}\right)V_{\mathrm{dc}}} = \sqrt{\frac{3}{2}}\frac{yS_{\mathrm{RSS}}\cos\theta}{V_{\mathrm{LL,rms}}N_{\mathrm{dc,Cn}}} \qquad (20)$$

$$i_{\mathrm{Cn,ac}} = \frac{\sqrt{3}(1-y)S_{\mathrm{RSS}}\cos\theta}{(N_{\mathrm{ac,Cn}})V_{\mathrm{LL,rms}}} \qquad (21)$$

The power loss in the cable conductors is given by (22),

$$P_{\mathrm{cond,Cn}} = N_{\mathrm{ac,Cn}}i_{\mathrm{Cn,ac}}^2 Lr_{\mathrm{Cn,ac}}(T_{\mathrm{Cn,ac}}, A_{\mathrm{con}})$$
$$+ N_{\mathrm{dc,Cn}}i_{\mathrm{Cn,dc}}^2 Lr_{\mathrm{Cn,dc}}(T_{\mathrm{Cn,dc}}, A_{\mathrm{con}}) \qquad (22)$$

Substituting the value of conductor current from (21) and simplifying,

$$P_{\text{cond,Cn}} = 3L \left(\frac{(1-y)^2 r_{\text{Cn,ac}}(T_{\text{Cn,ac}}, A_{\text{con}})}{N_{\text{ac,Cn}}} + \frac{y^2 r_{\text{Cn,dc}}(T_{\text{Cn,dc}}, A_{\text{con}})}{2 \cdot N_{\text{dc,Cn}}} \right) \left(\frac{S_{\text{RSS}} \cos\theta}{V_{\text{LL,rms}}} \right)^2 \quad (23)$$

Here, $r_{\text{Cn,ac}}(T_{\text{Cn,ac}}, A_{\text{con}})$ and $r_{\text{Cn,dc}}(T_{\text{Cn,dc}}, A_{\text{con}})$ are the per km operating ac and dc resistances respectively, corresponding to temperatures $T_{\text{Cn,ac}}$ and $T_{\text{Cn,dc}}$, imposed by the operating currents $i_{\text{Cn,ac}}$ and $i_{\text{Cn,dc}}$ computed iteratively based on (9) and (10).

The converter losses $P_{\text{conv,Cn}}$ are described by (24)

$$P_{\text{conv,Cn}} = S_{\text{RSS}}[(1 - \eta_{\text{SSS}})y \cos\theta + (1 - \eta_{\text{RSS}})\sqrt{y^2 \cos^2\theta + \sin^2\theta}] \quad (24)$$

These are lower than that for C1 (see (18)) because the operating value of y governing the converter demands is lower than 1 and can be set between the range described by (7) and (8). The total system loss $P_{\text{loss,Cn}}$ in parallel ac-dc configuration can be estimated from conduction and converter losses similar to (19).

G. Crossover Lengths

Crossover length (L_{cr}) can be defined as the link length for which losses of any two configurations is equal. Theoretically, the configurations with N_{ori} link conductors can have $\frac{(\frac{N_{\text{ori}}}{3})(\frac{N_{\text{ori}}}{3}+1)}{2}$ crossover points, with the constraint $L_{\text{cr}} > 0$. The relevant crossover points are those that describe the lowest system losses as a function of link length. The L_{cr} for any two given configurations can be derived by equating the relevant system loss equations derived in Section II-F. By equating (19) and (14) and simplifying, the crossover ($L_{\text{cr,C0C1}}$) between C0 and C1 can be found from (25).

$$L_{\text{cr,C0C1}} = \frac{P_{\text{conv,C1}}}{3\left(\frac{r_{\text{C0}}}{N_{\text{ori}}+3} - \frac{\cos^2\theta r_{\text{C1}}}{2N_{\text{dc,C1}}}\right)} \left(\frac{V_{\text{LL,rms}}}{S_{\text{RSS}}}\right)^2 \quad (25)$$

Similarly, the crossover of parallel ac-dc link (Cn with n≠(0,1)) with C0 ($L_{\text{cr,C0Cn}}$) and C1 ($L_{\text{cr,C1Cn}}$) can be found using (26) and (27) respectively.

$$L_{\text{cr,C0Cn}} = \frac{P_{\text{conv,Cn}} \left(\frac{V_{\text{LL,rms}}}{S_{\text{RSS}}}\right)^2}{3\left(\frac{r_{\text{C0}}}{N_{\text{ori}}+3} - \cos^2\theta \left(\frac{(1-y)^2 r_{\text{C2,ac}}}{N_{\text{ac,Cn}}} + \frac{y^2 r_{\text{C2,dc}}}{2N_{\text{dc,Cn}}}\right)\right)} \quad (26)$$

$$L_{\text{cr,C1Cn}} = \frac{(P_{\text{conv,C1}} - P_{\text{conv,Cn}}) \left(\frac{V_{\text{LL,rms}}}{S_{\text{RSS}}}\right)^2}{3\cos^2\theta \left(\frac{(1-y)^2 r_{\text{C2,ac}}}{N_{\text{ac,Cn}}} + \frac{y^2 r_{\text{C2,dc}}}{2N_{\text{dc,Cn}}} - \frac{r_{\text{C1}}}{2N_{\text{dc,C1}}}\right)} \quad (27)$$

H. Economic Analysis

Even though each configuration can maintain the same power delivery capacity during (n-1) contingencies, the installation costs incurred in their realization is different. For C0, link length dependent cost $f_{\text{c,C0}}(L)$ is incurred in procuring, digging and installation of an additional 3-phase cable link. Based on feedback from experts associated with the DNOs (see Acknowledgements), a ballpark value can be assumed between 100-200 €/m in The Netherlands. However, these figures are only indicative and location-specific.

On the other hand, the refurbished dc based configuration costs ($f_{\text{c,Cn}}$ for n≠0,1) include converter costs (assumed 50 €/kVA based on [30]) $f_{\text{c,conv}}(S_{\text{rated,RSS}}, S_{\text{rated,SSS}})$, where $S_{\text{rated,RSS}}$ and $S_{\text{rated,SSS}}$ are the substation converter rating at RSS and SSS sides, given by (11) and (12) respectively at full load. From the equations, it can be inferred that since the value of y is lower than 1 for parallel ac-dc configurations (Cn where n≠(0,1)), the corresponding costs are lower as compared to C1. Furthermore, each converter station space requirements can be assumed at 50000 €. It can be inferred that the costs for refurbished dc configurations is independent of link length.

These cost functions are used to compute the payback due to the savings associated with the losses of one configuration as compared to other. The energy savings are translated to €s using a unit cost of 0.1 €/kWh [4]. These aspects shall be explored in Section V.

III. EFFICIENCY BOUNDARIES FOR DIFFERENT CONFIGURATIONS

A. System Paramters and Key Assumptions

In this section the efficiency boundaries are derived for different configurations (C0-C3) using a case-study with $N_{\text{ori}} = 9$. The presented results correspond to the system parameters described in Table II.

TABLE II: System Parameters

$V_{\text{LL,rms}}$	10 kV
Type of conductor	Aluminum
A_{con}	400 mm^2
Rated conductor current	450 A
Average converter efficiency	99.34 %
Capacity during (n-1) contingencies	3 p.u.
Base Power	7.8 MVA

The base power corresponds to S_{link} and will change for the sensitivity analysis in Section IV showing the variation in the defined boundaries in accordance with the associated parameters. The key assumptions are as follows:

- The dc link voltage given by (16) corresponds to a conservative estimate of the cable insulation performance when refurbished from ac to dc operation [25]. Some studies suggest that this value can be increased to some extent for cables [5] and can be significantly higher for overhead lines [7], [8]. Further, depending on the operating boundaries of the converter, a slight increment in V_{dc} may be necessary. Any increase in V_{dc} will change

the (n-1) capacity constraints, influence the converter cost and reduce the dc link conductor loss for the given power.

- All 9 system link conductors are single-cored cables. While efficiency boundaries may not shift with three-cored cables of the same A_{con}, reliability considerations for minimum capacity during (n-1) contingencies may be different [13].
- The dc link with back-to-back MMCs forms a symmetric monopole system where the RSS-side converter is designed to deliver the full reactive power demand.
- The efficiency curve shown in Fig. 2 is adapted corresponding to the percentage loading of a single MMC per substation fully rated for the required dc link power. If multiple partially rated converters are employed to deliver the dc link power, this can influence the cost and reliability of the system. Further, depending on the load sharing between such converters, the efficiency curve may be made flatter, particularly at light loading conditions.

B. System Losses and Crossover Points

Based on the power loss equations derived in the previous section, the link length dependent system losses are shown in Fig. 3 for different strategies C0-C3 delivering $S_{RSS} = 3\,\text{p.u}$ at pf=0.9. The depicted losses are normalized with respect to S_{RSS}. The dc active power share y is considered 0.75 for C2 and 0.33 for C3.
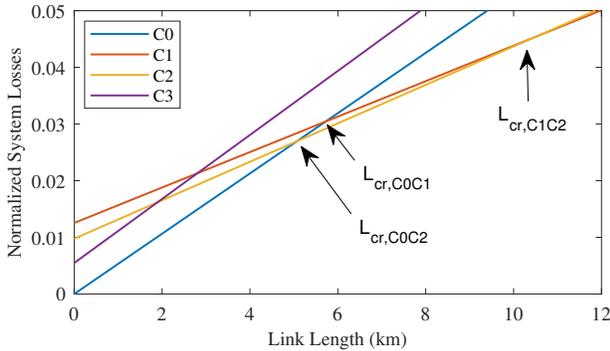

Fig. 3: Link length dependent normalized system power losses for different operational mode strategies.

It can be observed that when a parallel ac-dc configuration such as C2/C3 is used, these losses are lower than C1 as a part of S_{RSS} is delivered using the ac link. The system losses are highest for C0 after crossover points $L_{cr,C0C1}$ and $L_{cr,C0C2}$ as compared to C1 and C2 respectively, which can be described by (25) and (26). This is because the ac conductor losses are higher than that for dc, mainly due to lower link voltage, and these dominate the system losses over the fixed converter losses as the link length increases beyond the crossover points. Similarly, C2 becomes less efficient as compared to C1 after crossover point $L_{cr,C1C2}$ as described by (27). Configuration C3 is not the most efficient at any link length in this example, and thus its role will not be further explored in describing the efficiency boundaries. However, this configuration can offer some operational advantages along with the possibility to reduce converter costs as discussed in [13].
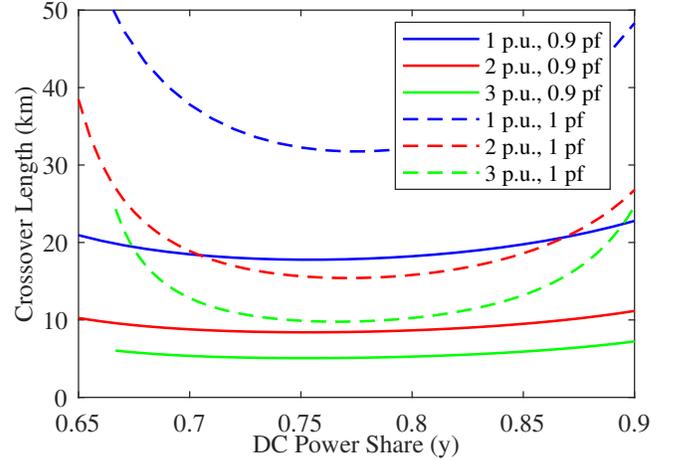
(a)
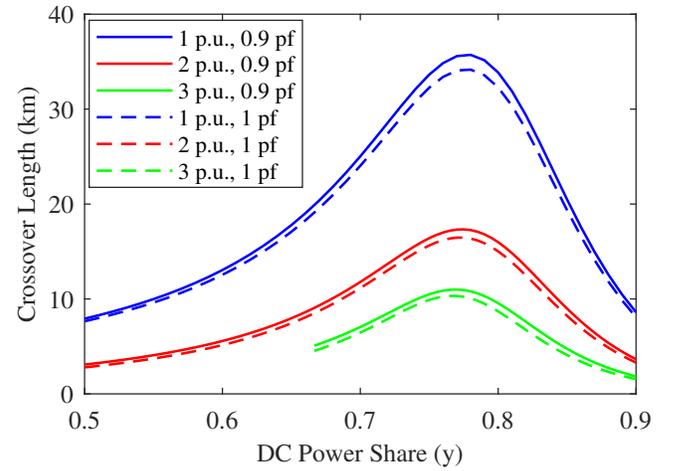
(b)

Fig. 4: Variation of crossover lengths with y for different S_{RSS} and pf (a) $L_{cr,C0C2}$ (b) $L_{cr,C1C2}$.

Equations (25)-(27) suggest that even if the system parameters are fixed according to Table II, the crossover points can vary depending on the operating conditions such as S_{RSS}, pf and y. Therefore, a proper knowledge of these dependencies are necessary to define the efficiency boundaries based on the expected operating conditions of the system over its lifetime.

C. Variation in Crossover Lengths with Operating Conditions

In Fig. 4, the variation in the crossover lengths is shown as y varies between the range y_{min} to y_{max} for configuration C2. The main observation is that in any considered scenario, preference for a parallel ac-dc link configuration has a optimal value with respect to the set value of operating y. Furthermore, the crossover length decreases with increasing S_{RSS}, consistent with (26) and (27).

Specifically, Fig. 4a indicates a minimum $L_{cr,C0C2} = L_{C2,min}$ at $y =\approx 0.75$. If the operating point is shifted by $\pm\Delta y$, the incurred losses in C2 are higher, mainly because the corresponding $P_{cond,C2}$ increases due to the uneven distribution of conductor currents in the ac and dc links. The influence of
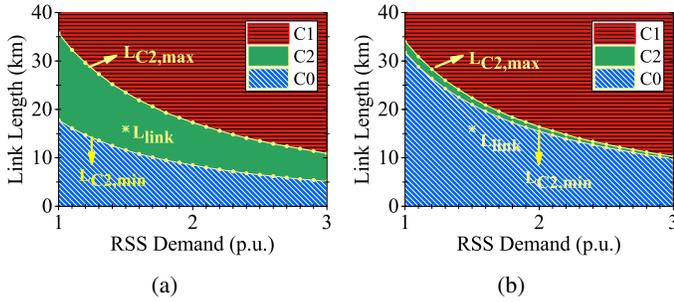
Fig. 5: Optimal efficiency configuration corresponding to link length and RSS power demand at (a) pf=0.9 (b) pf=1.

converter losses also play a role to determine the exact optimal point. Similar principle can be applied to explain the maximum $L_{cr,C1C2} = L_{C2,max}$ in Fig. 4b. As observed, the optimal point varies with the S_{RSS}, pf as well as link length and the minimum and maximum attainable values $L_{C2,min}$ and $L_{C2,max}$ for the given S_{RSS} and pf can be determined from Fig. 4a and Fig. 4b respectively.

D. Efficiency Boundaries

For a system described by the parameters in Table II, the appropriate choice of the configuration (C_{apt}) varies with the given link length L_{link} and the operating conditions. For the studied case, only two relevant crossovers define C_{apt} as per (28).

$$C_{apt} = \begin{cases} C_0, & \text{if } (L_{link} < L_{C2,min}) \\ C_1, & \text{if } (L_{link} > L_{C2,max}) \\ C_2, & \text{if } (L_{link} \geq L_{C2,min}) \wedge (L_{link} \leq L_{C2,max}) \end{cases} \quad (28)$$

The maximum efficiency boundaries for selecting the operational configuration specific to the normalized RSS demand S_{RSS}/S_{link}, pf and link length between SSS and RSS are shown in Fig. 5.

From Fig. 5a, it can be observed that the boundary $L_{C2,min}$ at which a shift in C_{apt} occurs from configuration with only ac links (C0, blue) to a parallel ac-dc link operation (C2, green) decreases as the power demand increases. A similar trend with demand is observed in the shift from C2 (green) to pure dc operation (C1, red) at boundary $L_{C2,max}$. It can be inferred that as S_{RSS} increases, preference for dc based power delivery for a given L_{link} increases. For example, C2 is the most efficient configuration for the depicted point $L_{link}(1.5,16)$. However, if the demand is 3 p.u, C1 is more efficient, while, C0 is more efficient if the demand is 1 p.u. Another important observation from Fig. 5a is that the efficiency range ($\Delta L_{link} = L_{C2,max} - L_{C2,min}$) for C2 increases with decrease in S_{RSS}. Also, Fig. 5b depicts that ΔL_{link} is relatively lower if the operating pf=1.

In conclusion, this section shows that the parallel ac-dc link based power delivery is relatively the most efficient configuration within a defined window of link lengths that expands with decreasing RSS demand and power factor.

IV. SENSITIVITY ANALYSIS WITH VARIOUS INFLUENCING FACTORS

The previous section defines the efficiency boundaries of parallel ac-dc link configuration C2 for the link lengths bounded by $L_{C2,min}$ and $L_{C2,max}$ with varying operating conditions specific to a system with parameters listed in Table II. This section provides the sensitivity analysis of the defined boundary with varying grid voltage, link conductor area and converter efficiency. During the sensitivity analysis corresponding to a particular variable, the values of all other parameters is the same as Table II, unless otherwise specified.

A. AC Substation Voltage

Figure 6 shows that the region bounded by the surfaces representing $L_{C2,max}$ and $L_{C2,min}$ increase with $V_{LL,rms}$ (x-axis) and S_{RSS} (y-axis). C2 is the most efficient configuration for any system with link length L_{link} operating in this region.
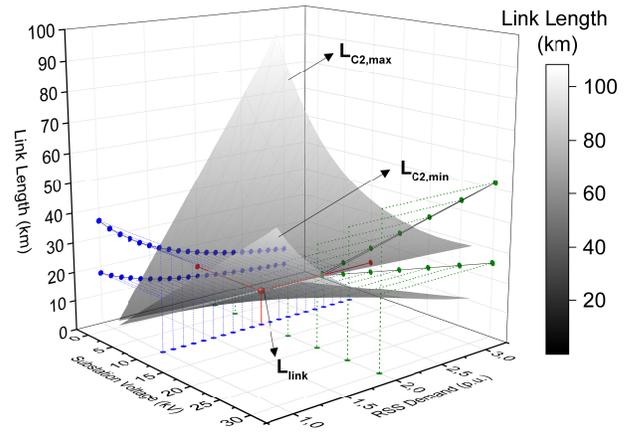

Fig. 6: Sensitivity of C2 efficiency boundary to $V_{LL,rms}$ (x-axis) with varying operating S_{RSS} (y-axis) at pf=0.9.

The projection of the two surfaces in the YZ plane at $V_{LL,rms} = 10\,\text{kV}$ corresponds to the 2D representation of the same operating condition shown in Fig. 5a. The projection of the surfaces in the XZ-plane at $S_{RSS} = 2\,\text{p.u}$ shows that $L_{C2,min}$ and $L_{C2,max}$ linearly increase with grid voltage. This is consistent with the direct-square relationship mathematically predicted in (26) and (27) because the base power (S_{link}) used to normalize the depicted S_{RSS} also proportionally increases with $V_{LL,rms}$. Fig. 7 shows the XZ-projection of Fig. 6 for different power demands.

The main conclusion is that the efficiency range of C2 expands with increasing grid voltage but the bounded region occurs at higher link lengths for a given S_{RSS}.

B. Conductor Area

Fig. 8 shows the efficiency boundary surfaces $L_{C2,min}$ and $L_{C2,max}$ with varying A_{con} (x-axis) and S_{RSS} (y axis). C2 is the most efficient configuration for any system with link length L_{link} operating within this bounded region.
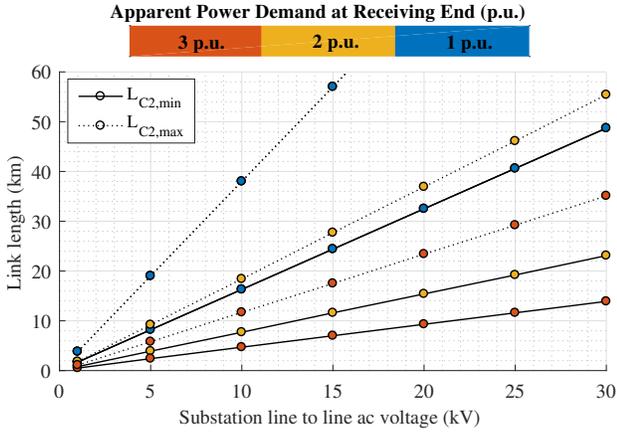
Fig. 7: Influence of $V_{LL,rms}$ on $L_{C2,min}$ and $L_{C2,max}$ for different apparent power demands.
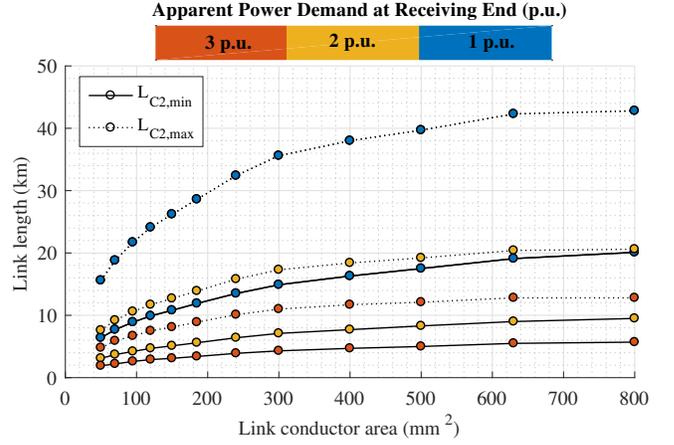

Fig. 9: Influence of A_{con} on $L_{C2,min}$ and $L_{C2,max}$ for different apparent power demands.
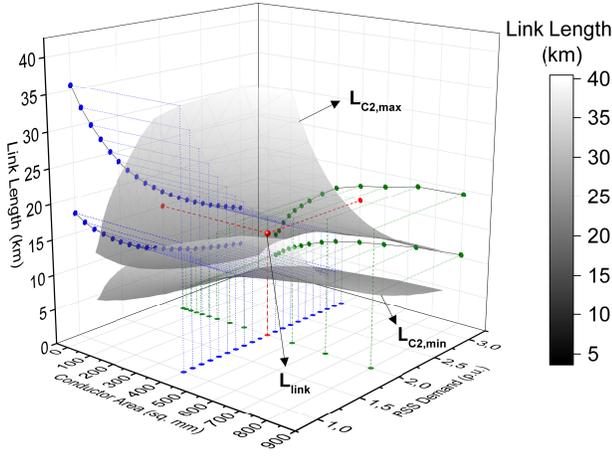

Fig. 8: Sensitivity of C2 efficiency boundary to A_{con} (x-axis) with varying operating S_{RSS} (y-axis) at pf=0.9.

of converters per substation. Furthermore, even for a given converter station design, the efficiency can dynamically vary with loading as a percentage of rating corresponding to Fig. 2. Fig. 10 offers a generic insight on the variation in the surfaces $L_{C2,min}$ and $L_{C2,max}$ with varying efficiency (x-axis) corresponding to any possible demand (y-axis).
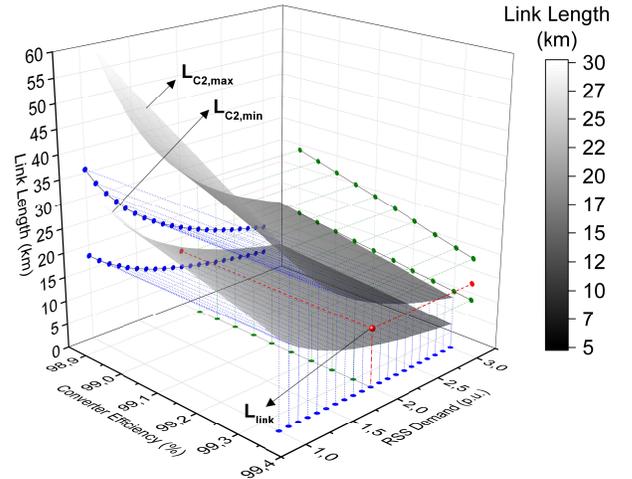

Fig. 10: Sensitivity of C2 efficiency boundary to converter station efficiency (x-axis) with varying operating S_{RSS} (y-axis) at pf=0.9.

The base power S_{link} used to normalize the actual MVA demand S_{RSS} increases with cross-sectional area due to a corresponding increase in the rated current carrying capability of the conductor. The YZ-plane projection at $A_{con} = 400\,mm^2$ corresponds to the 2D representation of the same operating condition as Fig. 5a. The XZ-plane projection shows the variation of $L_{C2,min}$ and $L_{C2,max}$ with A_{con} at $S_{RSS} = 2\,p.u.$ Mathematically, the relationship is described by the corresponding variation in the ac and dc link conductor resistances in (26) and (27). Fig. 9 shows the XZ-projection of Fig. 8 for different power demands.

The main conclusion is that the efficiency range of C2 expands with increasing A_{con}, however, the bounded region occurs at higher link lengths for a given S_{RSS}.

C. Substation Converter Efficiency

Thus far, results are presented by assuming a flat efficiency curve for MMC at 99.34 %. However, the substation efficiency can vary with converter design, rating as well as number

For example, if the $S_{RSS} = 2\,p.u$, the value of $L_{C2,min}$ and $L_{C2,max}$ for any possible converter efficiency can be estimated from the XZ-projection. The observed relationship is consistent with the analytical expression derived in (26) and (27). Similarly, the slice of the surface plot at 99.34 % projected onto the YZ-plane shows the variation with S_{RSS}, consistent with the result in Fig. 5a. Fig. 11 shows the XZ-projection of Fig. 10 for different power demands.

Therefore, C2 is the most efficient configuration if the system with link length L_{link} exists in the region bounded within the surfaces $L_{C2,min}$ and $L_{C2,max}$ for the possible operating power and converter efficiency.
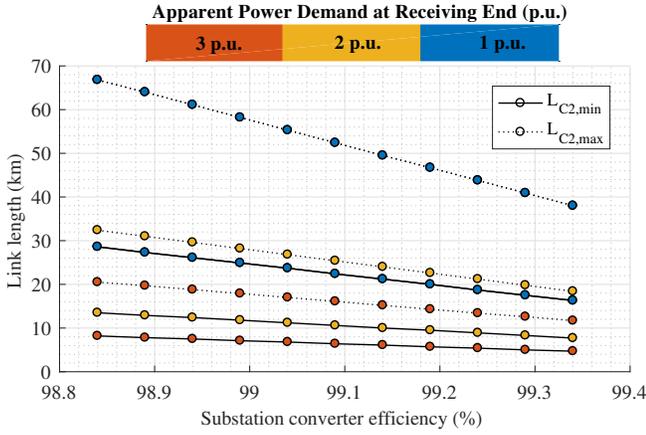
Fig. 11: Influence of converter efficiency on $L_{C2,min}$ and $L_{C2,max}$ for different apparent power demands.

V. ECONOMIC CONSIDERATIONS

In this section, the economic viability boundaries of the configurations for the system corresponding to the case-study in Section III will be described based on the assumptions highlighted in Section II-H. The considered converter cost is 50 €/kVA, while that of laying an additional 3-phase ac cable link is 100 €/m; a sensitivity analysis to the economic viability considerations corresponding to these parameters will be explored. Let $L_{10,C0\text{-}C2}$ be the link length for which the payback period of additional investment of C2 over C0 $(f_{c,C2} - f_{c,C0})$ is 10 years. Also, let $L_{10,C1\text{-}C2}$ be the link length for which the payback period of additional investment of C2 over C1 $(f_{c,C2} - f_{c,C1})$ is 10 years. Then, the region enclosed by $L_{10,C0\text{-}C2}$ and $L_{10,C1\text{-}C2}$ describes the economic viability for configuration C2. This economic viability region is overlayed upon the efficiency boundaries in Fig. 5a and depicted in Fig. 12.

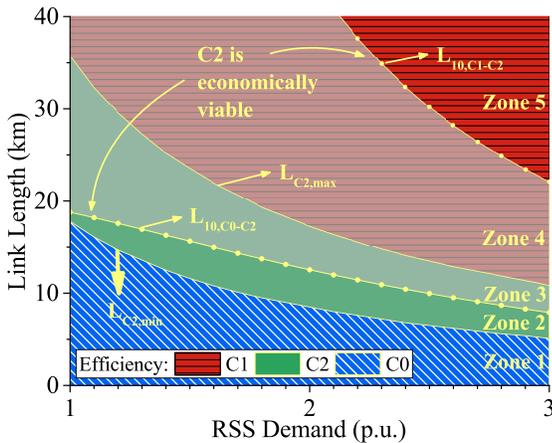

Fig. 12: C2 economic viability boundary for a 10 year payback period with varying link lengths and RSS demand at pf=0.9.

It can be observed that the plot lines $L_{C2,min}$, $L_{C2,max}$, $L_{10,C0\text{-}C2}$ and $L_{10,C1\text{-}C2}$ segregate the area plot into 5 zones. Each zone corresponds to a different efficiency and economic

viability combinations of possible configurations as shown in Table III.

TABLE III: Viability Zones for Different Configurations

Zone	1	2	3	4	5
Most Efficient	C0	C2	C2	C1	C1
Economically viable	C0	C0	C2	C2	C1

Zone 4 is the most interesting as it indicates that even though a system with only dc links (C1) is the most efficient in this region, the parallel ac-dc configuration (C2) can be a more economically viable choice. This is because even though the system has the same power delivery capacity during (n-1) contingencies, the required converter rating is lower for C2. The main conclusion is that configuration C2 is the ideal choice for a system with any link length in the region comprising (Zone 3) ∪ (Zone 4) within the operating conditions depicted for the parameters listed in Table II. In this region, it will also be relatively more efficient than a solely ac link configuration (C0).

If the converter costs are reduced from 50 €/kVA to 25 €/kVA, it can be expected that the converter station costs of both configurations C1 and C2 will proportionally reduce. Consequently, the plot curves for $L_{10,C0\text{-}C2}$ and $L_{10,C1\text{-}C2}$ will shift downwards by a negative y-offset as shown in Fig. 13. It can be observed that all zones except Zone 2 represent the same efficiency and economic viability boundaries as Table III, albeit at different operating conditions and link lengths.
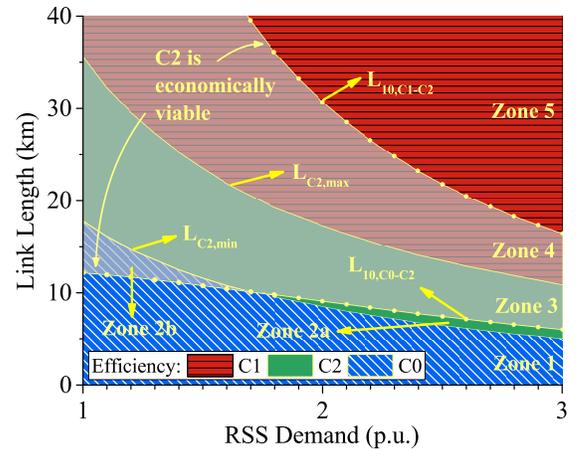

Fig. 13: Sensitivity of C2 economic viability boundary to reduced converter price of 25 €/kVA with varying link lengths and RSS demand at pf=0.9.

Zone 2a represents the region where C2 is more efficient but the payback on the additional investment as compared to C0 is greater than 10 years. In Zone 2b, C0 is the most efficient configuration but the additional investment in installing a new ac link does not recover within the considered 10 year payback time. Therefore, C2 should be the preferred solution in regions comprising (Zone 2b) ∪ (Zone 3) ∪ (Zone 4). The main conclusion is that if the converter costs reduce, the economic viability of parallel ac-dc link configuration will increase at comparatively shorter link lengths.

Fig. 14 shows that if the considered cost of installing an additional underground 3-phase ac link is increased from 100 €/m to 200 €/m, the plot line corresponding to $L_{10,C0-C2}$ shifts downwards by a negative y-offset as compared to Fig. 12. However, the curve-line described by $L_{10,C1-C2}$ remains the same. Thus, it can be inferred that if the considered link conductor installation costs are higher, the region of economic viability of refurbished parallel ac-dc links expand, particularly to include relatively lower link lengths.
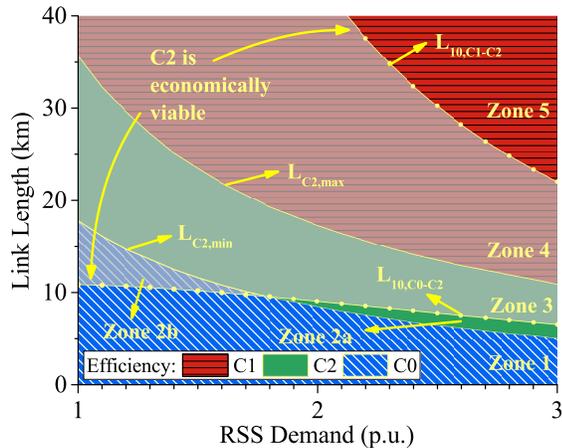

Fig. 14: Sensitivity of C2 economic viability boundary to link conductor installation cost of 200 €/m with varying link lengths and RSS demand at pf=0.9.

VI. CONCLUSIONS

Different configurations, using ac to dc refurbishment concept, were compared in terms of the operating efficiency and economic viability for different power demands, power factors, dc link power share and link length, with respect to the conventional ac capacity enhancement solution. The paper builds from the premise that the studied system configurations can maintain the same power delivery capacity during (n-1) contingency. To achieve this capacity, the configuration with only ac links have incurred costs for installing additional link conductors and that with only refurbished dc links have full load converter costs. On the other hand, refurbished parallel ac-dc link configurations can reduce the converter costs by maintaining the required capacity using reconfiguration.

The main finding of this paper is that a refurbished parallel ac-dc configuration can offer superior efficiency as compared to configurations with, solely, either ac or dc links, within a certain operating range. Based on the derived analytic equations, these efficiency boundaries were defined for a case-study. It was shown that within a window of relatively short link lengths the parallel ac-dc configuration (C2) is the most efficient, and this region expands with decreasing delivered power and power factor.

Sensitivity analysis suggests that the region in which C2 is relatively more efficient expands with increasing grid voltage, increasing link conductor area and decreasing converter efficiency. However, the link length coordinates for the surfaces

by which this region is bound, consequently increases for given operating power, thus implying that the equivalent efficiency is achieved at longer link lengths.

The economic viability region of C2 does not completely overlap with its efficiency boundary and is relatively wider for the given RSS demand. The study suggests that the parallel ac-dc link configuration can be a favoured economic choice as compared to a system with only dc links for the defined zones because of lower converter costs even if the efficiency is not necessarily higher. A sensitivity analysis with decreased converter cost as well as increased link conductor installation cost can shift the economic viability window of C2 towards lower lengths for given operating power.

Therefore, the main conclusion is that refurbished parallel ac-dc reconfigurable distribution links can be an efficient and economically preferred possibility, particularly for delivering high power (few tens of MVA) at medium voltage levels (one to few tens of kV) for short distances (0-50 km).

REFERENCES

[1] A. Rentschler, G. Kuhn, M. Delzenne, and O. Kuhn, "Medium voltage dc, challenges related to the building of long overhead lines," in *IEEE Transmission & Distribution*, April 2018, pp. 1–5.

[2] A. Shekhar, L. Ramírez-Elizondo, X. Feng, E. Kontos, and P. Bauer, "Reconfigurable dc links for restructuring existing medium voltage ac distribution grids," *Electric Power Components and Systems*, vol. 45, no. 16, pp. 1739–1746, 2017.

[3] S. K. Chaudhary, J. M. Guerrero, and R. Teodorescu, "Enhancing the capacity of the ac distribution system using dc interlinks x2014;a step toward future dc grid," *IEEE Transactions on Smart Grid*, vol. 6, no. 4, pp. 1722–1729, July 2015.

[4] A. Shekhar, E. Kontos, L. Ramírez-Elizondo, A. Rodrigo-Mor, and P. Bauer, "Grid capacity and efficiency enhancement by operating medium voltage ac cables as dc links with modular multilevel converters," *International Journal of Electrical Power Energy Systems*, vol. 93, pp. 479 – 493, 2017.

[5] Y. Liu, X. Cao, and M. Fu, "The upgrading renovation of an existing xlpe cable circuit by conversion of ac line to dc operation," *IEEE Transactions on Power Delivery*, vol. 32, no. 3, pp. 1321–1328, June 2017.

[6] L. Zhang, J. Liang, W. Tang, G. Li, Y. Cai, and W. Sheng, "Converting ac converting ac distribution lines to dc to increase transfer capacities and dg penetration," *IEEE Transactions on Smart Grid*, pp. 1–1, 2018.

[7] D. M. Larruskain, I. Zamora, O. Abarrategui, and Z. Aginako, "Conversion of ac distribution lines into dc lines to upgrade transmission capacity," *Electric Power Systems Research*, vol. 81, no. 7, pp. 1341 – 1348, 2011.

[8] A. Clerici, L. Paris, and P. Danfors, "Hvdc conversion of hvac lines to provide substantial power upgrading," *IEEE Transactions on Power Delivery*, vol. 6, no. 1, pp. 324–333, Jan 1991.

[9] K. Sharifabadi, L. Harnefors, H.-P. Nee, S. Norrga, and R. Teodorescu, "Design, control, and application of modular multilevel converters for hvdc transmission systems," *Wiley*, Oct 2016.

[10] E. Kontos, G. Tsolaridis, R. Teodorescu, and P. Bauer, "High order voltage and current harmonic mitigation using the modular multilevel converter statcom," *IEEE Access*, vol. 5, pp. 16 684–16 692, 2017.

[11] ——, "On dc fault dynamics of mmc-based hvdc connections," *IEEE Transactions on Power Delivery*, vol. 33, no. 1, pp. 497–507, Feb 2018.

[12] A. Shekhar, E. Kontos, L. Ramírez-Elizondo, and P. Bauer, "Ac distribution grid reconfiguration using flexible dc link architecture for increasing power delivery capacity during (n-1) contingency," *IEEE Southern Power Electronics Conference (SPEC)*, 2017.

[13] A. Shekhar, L. Ramírez-Elizondo, and P. Bauer, "Reliability, efficiency and cost trade-offs for medium voltage distribution network expansion using refurbished ac-dc reconfigurable links," *IEEE 24th International Symposium on Power Electronics, Electrical Drives, Automation and Motion (SPEEDAM)*, 2018.

[14] H. A. Peterson, D. K. Reitan, and A. G. Phadke, "Parallel operation of ac and dc power transmission," *IEEE Transactions on Power Apparatus and Systems*, vol. 84, no. 1, pp. 15–19, Jan 1965.

[15] H. Rahman and B. H. Khan, "Power upgrading of transmission line by combining ac ndash;dc transmission," *IEEE Transactions on Power Systems*, vol. 22, no. 1, pp. 459–466, Feb 2007.

[16] J. Reeve and E. Uzunovic, "Study of power transfer capability of dc systems incorporating ac loads and a parallel ac line," *IEEE Transactions on Power Delivery*, vol. 12, no. 1, pp. 426–434, Jan 1997.

[17] D. Jovcic and K. Ahmed, "High voltage direct transmission: Converters, systems and dc grids," *Wiley*, Sep 2015.

[18] H. M. A. Ahmed, A. B. Eltantawy, and M. M. A. Salama, "A generalized approach to the load flow analysis of ac 8211;dc hybrid distribution systems," *IEEE Transactions on Power Systems*, vol. 33, no. 2, pp. 2117–2127, March 2018.

[19] J. m. Maza-Ortega, A. Gomez-Exposito, M. Barragan-Villarejo, E. Romero-Ramos, and A. Marano-Marcolini, "Voltage source converter-based topologies to further integrate renewable energy sources in distribution systems," *IET Renewable Power Generation*, vol. 6, no. 6, pp. 435–445, November 2012.

[20] R. T. Pinto, M. Arags-Pealba, O. Gomis-Bellmunt, and A. Sumper, "Optimal operation of dc networks to support power system outage management," *IEEE Transactions on Smart Grid*, vol. 7, no. 6, pp. 2953–2961, Nov 2016.

[21] S. I. Nanou, G. N. Psarros, S. A. Papathanassiou, and M. P. Papadopoulos, "Operating reserve scheduling for island systems with parallel ac-dc interconnectors: The case of crete," in *2017 IEEE Manchester PowerTech*, June 2017, pp. 1–5.

[22] S. I. Nanou and S. A. Papathanassiou, "Frequency control of island vsc-hvdc links operating in parallel with ac interconnectors and onsite generation," *IEEE Transactions on Power Delivery*, vol. 33, no. 1, pp. 447–454, Feb 2018.

[23] E. Kontos, T. Schultz, L. Mackay, L. R. Elizondo, C. M. Franck, and P. Bauer, "Multi-line breaker for hvdc applications," *IEEE Transactions on Power Delivery*, vol. PP, no. 99, pp. 1–1, 2017.

[24] E. Kontos, R. T. Pinto, S. Rodrigues, and P. Bauer, "Impact of hvdc transmission system topology on multiterminal dc network faults," *IEEE Transactions on Power Delivery*, vol. 30, no. 2, pp. 844–852, April 2015.

[25] A. Shekhar, X. Feng, A. Gattozzi, R. Hebner, D. Wardell, S. Strank, A. Rodrigo-Mor, L. Ramírez-Elizondo, and P. Bauer, "Impact of dc voltage enhancement on partial discharges in medium voltage cablesan empirical study with defects at semicon-dielectric interface," *Energies*, vol. 10, no. 12, 2017.

[26] R. Alvarez, M. Wahle, H. Gambach, and J. Dorn, "Optimum semiconductor voltage level for mmc submodules in hvdc applications," in *2016 18th European Conference on Power Electronics and Applications (EPE'16 ECCE Europe)*, Sept 2016, pp. 1–9.

[27] J. E. Huber and J. W. Kolar, "Optimum number of cascaded cells for high-power medium-voltage ac-dc converters," *IEEE Journal of Emerging and Selected Topics in Power Electronics*, vol. 5, no. 1, pp. 213–232, March 2017.

[28] A. Shekhar, T. B. Soeiro, Z. Qin, L. Ramírez-Elizondo, and P. Bauer, "Suitable submodule switch rating for modular multilevel converter design in medium voltage applications," *IEEE Energy Conversion Congress and Exposition (ECCE)*, 2018.

[29] S. Rodrigues, A. Papadopoulos, E. Kontos, T. Todorcevic, and P. Bauer, "Steady-state loss model of half-bridge modular multilevel converters," *IEEE Transactions on Industry Applications*, vol. 52, no. 3, pp. 2415–2425, May 2016.

[30] R. W. D. Doncker, "Power electronic technologies for flexible dc distribution grids," in *2014 International Power Electronics Conference (IPEC-Hiroshima 2014 - ECCE ASIA)*, May 2014, pp. 736–743.

Aditya Shekhar received the M.Sc. (cum laude) degree in Electrical Power Engineering from the Delft University of Technology, Delft, The Netherlands, in 2015, where he is currently working toward the Ph.D. degree in DC Systems. He was a visiting researcher at University of Texas at Austin (USA) in 2016, where he studied partial discharge behaviour of cable insulation under high voltage. He was awarded the IDEA League Scholarship to work on his MSc thesis in ETH, Zurich in the High Voltage Laboratory. He was given an honors degree for his internship work in TNO, The Netherlands in the field of solar roads and wireless energy transfer. He completed his undergraduate bachelor degree in Electrical with distinction in 2010 from National Institute of Technology, Surat, India.

Dr. Laura Ramírez-Elizondo is assistant professor at the DC Systems, Energy Conversion & Storage group. In 2003, she received her bachelors degree in Electrical Engineering and her bachelors degree in Music with a major in Piano at the Universidad de Costa Rica. She graduated with honors from her M.Sc. studies in Electrical Power Engineering at Delft University of Technology in 2007. She holds a PhD in electrical engineering from the Delft University of Technology (2013).

Dr. Thiago Batista Soeiro (S10A11M11) received the B.S. (Hons.) and M.S. degrees in electrical engineering from the Federal University of Santa Catarina, Florianopolis, Brazil, in 2004 and 2007, respectively, and the Ph.D. degree from the Swiss Federal Institute of Technology, Zurich, Switzerland, in 2012. During the Master and Ph.D. studies, he was a Visiting Scholar at the Power Electronics and Energy Research Group, Concordia University, Montreal, QC, Canada, and at the Center for Power Electronics Systems, Blacksburg, VA, USA, respectively. From 2012 to 2013, he was a Researcher at the Power Electronics Institute, Federal University of Santa Catarina. Since 2013, he has been a Senior Scientist at the Corporate Research Center, ABB Switzerland Ltd., Baden-Dttwil, Switzerland. He is currently an Assistant Professor at the DC Systems, Energy Conversion and Storage Group, Delft University of Technology, Delft, The Netherlands. His research interests include advanced power converters and dc system integration.

Prof. Dr. Pavol Bauer is currently a full Professor with the Department of Electrical Sustainable Energy of Delft University of Technology and head of DC Systems, Energy Conversion and Storage group. He received Masters in Electrical Engineering at the Technical University of Kosice (85), Ph.D. from Delft University of Technology (95) and title prof. from the president of Czech Republic at the Brno University of Technology (2008) and Delft University of Technology (2016). He published over 72 journal and almost 300 conference papers in my field (with H factor Google scholar 32, Web of science 20), he is an author or co-author of 8 books, holds 4 international patents and organized several tutorials at the international conferences. He has worked on many projects for industry concerning wind and wave energy, power electronic applications for power systems such as Smarttrafo; HVDC systems, projects for smart cities such as PV charging of electric vehicles, PV and storage integration, contactless charging; and he participated in several Leonardo da Vinci and H2020 EU projects as project partner (ELINA, INETELE, E-Pragmatic) and coordinator (PEMCWebLab.com-Edipe, SustEner, Eranet DCMICRO).